Monitoring Toxic Gases Using Nanotechnology and Wireless Sensor Networks

Waltenegus Dargie, *Senior Member, IEEE*, Jianjun Wen, Luis Antonio Panes-Ruiz, Leif Riemenschneider, Bergoi Ibarlucea, Gianaurelio Cuniberti, *Senior Member, IEEE*

***Abstract*— Human beings live and work in close proximity to dangerous gases. Chemical accidents often cause considerable damages to human lives as well as properties and their short- and long-term impact on the environment can be high. Hence, diligent monitoring and management of these gases are of profound importance. In industries where chemical accidents pose potential explosions and health hazards, wired sensors are installed in strategic locations. In some industries, employees are required to carry with them portable sensing devices in addition. Still, achieving high spatio-temporal resolution is challenging, since dense deployments impede the mobility of employees, robots, or other mobile objects. In this paper, we propose the use of nanotechnology and wireless sensor networks for monitoring toxic gases. Nanotechnology offers the possibility of developing gas sensors having small form-factors and high sensitivity. Wireless sensor networks enable high spatio-temporal sensing, in-network processing, and multi-hop communications. The paper shares our experience with a wireless sensor network monitoring ammonia. The network consisted of 21 sensor nodes, four of which integrated arrays of ammonia sensors while the rest served as intermediate nodes.**

***Index Terms*— Ammonia, hydrogen sulphate, latency, monitoring, multihop communication, nanosensors, nanotechnology, response time, toxic gas detection, wireless sensor networks**

I. Introduction

Human beings often live and work in close proximity to dangerous gases. During oil exploration and refinery, toxic gases, such as ammonia and hydrogen sulfide, are produced as byproducts [1], [2]. The gases are useful for producing fertilizers, environment friendly refrigerants, explosives, munition plants, and pharmaceuticals [3], but they are also dangerous. Ammonia is a highly reactive, soluble alkaline gas which is lighter than air. If inhaled, it cauterizes respiratory tracts and can be fatal at concentrations above 5000 parts per million (ppm). Similarly, hydrogen sulphide is an extremely toxic and flammable gas which produces a rotten egg odor discernible at concentrations below 15 ppm.

Chemicals accidents cause human losses and damage to properties and their effect on the environment can be detrimental [4]. In 2021, a chemical accident in Ludwigshafen, Germany, caused an explosion and the release of 150 kg of methyl diethanolamine into the Rhein river [5]. Four years prior to this accident (in 2017) a pipeline explosion in the same industry killed three and seriously injured eight employees. At the time, the pipelines were transporting ethylene and propylene [6]. In 2015, a chemical industry in the Shandong province of China exploded, releasing a highly toxic gas (adiponitrile) into the environment; 215 people needed immediate medical treatment and 5 were injured seriously [7]. Cheung et al. [8], citing the National Census of Fatal Occupational Injuries survey conducted by the U.S. Bureau of Labor Statistics, observed that in 2015 there were 4836 workers killed on construction sites due to illness and fatalities – 9% of these were due to exposure to hazardous environment and 3%, due to fire and explosions. Perhaps, the most fateful chemical accident in history was the 1984 chemical factory accident in Bhopal, India, which spewed 40 tons of a toxic gas into the environment, causing a profound and long lasting health hazard to the city's inhabitants [9]. In 2015 the European commission published a list of accidents in chemical industries across Europe that year along with their causes, estimated damage, and the lessons learned [10]. In underground mining, employees are likewise exposed to dangerous gases and explosions sparked by coal-dust [11].

In industries where chemical accidents pose potential explosions and health hazards, wired sensors are installed in strategic locations. In some industries, employees are required to carry with them portable sensing devices in addition. Still, achieving high spatio-temporal resolutions is challenging, since dense deployments may impede the mobility of employees, robots, equipment, and other objects. Wireless sensor networks have several advantages. The nodes can be deployed easily and unobtrusively and their placement can be optimized based on experience and field observations. Similarly, network maintenance can be carried out without impending normal working conditions (and in some situations without involving human presence). Moreover, with the emergence of nanosensors, dense deployments can be supported to cover

Manuscript submitted on 16 September 2022.
This work has been partially funded by the Free State of Saxony under TG70 Research Funding program (Grant nummber: 100369691).
W. Dargie and J. Wen are with the Faculty of Computer Science, Technische Universität Dresden, 01062 Dresden, Germany (e-mail: {waltenegus.dargie, J. Wen}@tu-dresden.de)
L.A Panes-Ruiz, L. Riemenschneider, B. Ibarlucea, and G. Cuniberti are with Institute of Materials Science and Max Bergmann Center for Biomaterials, Technische Universität Dresden, 01062 Dresden, Germany (e-mail: {luis_antonio.panes_ruiz, leif.riemenschneider, bergoi.ibarlucea, gianaurelio.cuniberti}@tu-dresden.de)

extensive areas. But there are some challenges associated with wireless communications. Firstly, compared to wired links, wireless links are subject to interference and a high degree of packet loss. Secondly, the transmission range of wireless transceivers are limited which necessitates multi-hop communication. Multi-hop communication exacerbate packet loss and end-to-end packet transmission latency, thereby affecting the response time of the sensing system.

This paper proposes the use of nanotechnology and wireless sensor networks for monitoring toxic gases. Nanotechnology offers the possibility of developing gas sensors having small form-factors and high sensitivity. The sensing mechanism relies on the chemisorption and physisorption of gas molecules on the surface and interface of nano materials such as carbon nanotubes [12]. The wireless sensor network supports in-network processing (to reduce the network traffic density) and multi-hop communication. In our first prototype we focus on monitoring ammonia. The contributions of this papers are summarized as follows:

- Gas nanosensors with detection limits reaching 3 parts per billion (ppb).
- Wafer-scale compatible fabrication of small footprint (2.4 cm × 2.4 cm) devices consisting of 64 gas sensors.
- Low response time compared to commercially available ammonia sensors.
- A fully functional multi-hop wireless sensor network integrating arrays of nanosensors for monitoring ammonia.

The remaining part of this paper is organized as follows: In Section II related work is reviewed. In Section III, the development and integration of arrays of nanosensors are discussed. In Section IV, a mathematical model for data aggregation is presented. In Section V, the set up process and the performance of a wireless sensor network for monitoring ammonia is discussed. In Section VI the performance of the wireless sensor network is evaluated and comparison of results with state-of-the-art are discussed. Finally, in Section VII, concluding remarks are given and open issues are identified.

II. Related Work

Recent advances in processor, wireless, and sensor technologies promise high resolution, distributed, and autonomous monitoring of dangerous gases in various places.

Chang et al. [13] observe that as the level of pollution increases worldwide, the amount of volatile organic compounds and toxic inorganic gases populating the air increases, causing great harm to human life. One of these substances is aniline. Accordingly, when the body is exposed to aniline vapor, the skin, the digestive tract, and the respiratory tract absorb the gas. This may result in different health conditions, including methemoglobinemia, liver damage, and carcinogenesis. The authors developed a nanosensor to monitor aniline and integrated the sensor into a wearable device that fires an alarm when the surrounding aniline concentration passes a set threshold.

Perez et al. [14] propose a wireless sensor network for monitoring combustible and harmful concentrations of toxic gases as well as organic vapors, odorant, and amine in a shipyard. The main focus of the researchers, though, was on testing the performance of the sensor network in terms of its response time and reliability. Thus, the authors integrated off-the-shelf portable gas detectors (Dräger X-am 5000) into wireless sensor platforms and sampled the sensors every minute. Their analysis consisted of round trip time (RTT), packet error rate (PER) and link quality indicator (LQI) of the wireless links, taking into account the number of hops the packets needed to reach their destination. The robustness of the network and the response time of the overall system were analyzed from the point of view of a control station outside the shipyard. The packets needed up to 5-hop to reach the control station. Accordingly, RTT varied between 30 and 40 ms, and no packets were lost, except for the case of the longest hop, in which case the PER was 3%. The authors carried out in-ship tests, considering five different in-ship communication scenarios. In the first four, RTT, LQI and PER of representative internal single-hop links were measured. In the last scenario, they examined PER and RTT for a worst-case multi-hop path to monitor one of the ship holds, transmitting detector gas readings to a control station outside the vessel. In all the in-ship tests, node transmission power was set to its maximum value (20 dBm).

Asthana et al. [15] propose a wireless sensor network for monitoring the safety of sewage workers during cleaning and maintenance. The authors observe that septic tank gases may have concentrations of methane, carbon dioxide, sulfur dioxide, ammonia, hydrogen sulphide, nitrogen dioxide, and carbon monoxide, albeit with different intensities. Of these, the predominant are methane and carbon monoxide, which are also the target gases the authors aimed to monitor. The monitoring system is intended to immediately alert workers as well as a central station which closely examines the concentration and distribution of the gases and their long-term impact. In addition, the central station remotely calibrates all the gas sensors, adapt their sampling rates and intervals, and determines the appropriate threshold levels for septic plants and facilities. The authors integrated a commercially available gas sensor (MQ-4 gas sensor[1]), a CO sensor, and a temperature sensor into an Arduino Uno platform [16] and defined the following thresholds to fire an alarm: 2.3 ppm for CO and 60 ppm for methane. The CO sensor, in addition, measures the heat and motion of surrounding objects.

Cheung et al. [8] propose a system for monitoring toxic gases in construction sites. It consists of a control station, a sensing subsystem, and an actuating subsystem. The later includes a flash, an alarm system, and a ventilator to be activated in case of emergency. An actuating node controls these components. The sensing subsystem consists of gas and environmental sensors (temperature and humidity) as well as routers. Furthermore, the system was integrated with a building information modeling (BIM), an advanced technology in construction industry development to fuse different kinds of construction information into a 3D digital model. The BIM can be employed in all stages of a project life-cycle, such as planning, design, construction, operation and maintenance. The

[1]Hanwei Electronics (www.hwsensor.com).

integration enables to monitor the construction site visually and remotely via a spatial, colored interface. The system was deployed in north Taiwan, in a tunnel having a diameter of 5.6 m and a length of 528 m at a time when an actual underground construction was taking place. The deployment was intended to measure the response time of the system as a whole and the reliability of the wireless sensor network. The wireless sensors were placed with 100 m separation distance between them. The authors reported an impressive response time of 1-2 s. This time includes the detection of a gas concentration above a set threshold and an end-to-end packet transmission latency. Moreover, the system was able to alert the control station by indicating the abnormal condition on the tunnel's BIM. At the same time, the control node started the flash, the alarm, and the ventilator.

III. Nanosensors Integration

The accuracy with which toxic gases can be detected depends on the surface area to volume ratio of the sensor. Typically, gas detection takes place when gas molecules change the resistance of an underlying electric material in accordance with their atomic property and in proportion to the interaction intensity. Besides accuracy, sensitivity, selectivity, and response time are crucial, considering the magnitude of damage a gas leak can cause.

A. Technology

Our gas sensors are chemiresistors based on semiconducting single-walled carbon nanotubes (sc-SWCNTs) [17]. The sensing mechanism relies on the chemisorption and physisorption of the gas molecules on the surface of the nanotubes and the nanotube-electrode interface which modify the electrical properties of the system. The sensitivity provided by nanomaterials due to the high surface area to volume ratio is key, together with a fast response time and selectivity, considering the magnitude of damage a gas leak can cause. sc-SWCNTs in particular are known to respond more strongly to ammonia than to other gases [18]. Such response occurs due to the presence of free carboxyl acid functional groups on their surface, which are prone to interact with amine compounds [19]. In addition, nanotechnology has excellent features such as low power consumption, high electron transport, and mechanical properties allowing the fabrication of high sensitive sensors on flexible and lightweight supports. The later enables the mounting of the sensors on small robots and Unmanned Areal Vehicles (UAV) with low loading capacity.

In order to achieve a high sensitivity and a high spatial resolution, the sensing subsystem consists of an array of 64 chemiresistive sensors. The output of these sensors are multiplexed using four 16-channel, low leakage current multiplexers (ADG706), as shown in Fig. 1.[2] The selected current from each multiplexer is then fed to a transimpedance stage (TIA) based on IC LMP91000. The output voltage of the TIA is digitized using a low noise 24-bit ADC (ADS122C04) which is then supplied to a dedicated microcontroller (ESP32) via an I2C serial bus. The ADC is programmable at 2 ksps. Having a dedicated microcontroller is useful for separating the data processing (preprocessing) stage from other tasks (network management).

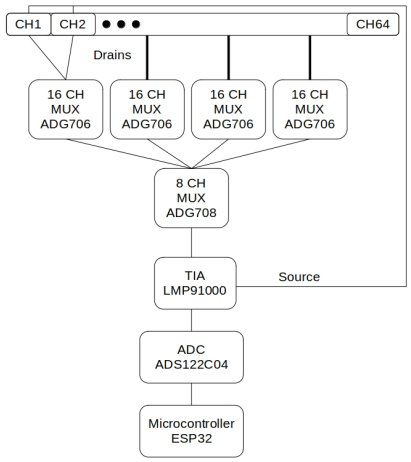

Fig. 1: The architecture of a 64-channel nanosensor for detecting ammonia and hydrogen sulfide.

Fig. 2: A wireless sensor node integrating an array of nanosensors for toxic gas detection and a Raspberry Pi and the Zolertia platform for network management.

B. System Integration

The sensing subsystem is interfaced with a Zolertia platform (RE-Motes[3]) via a Raspberry Pi board. The Zolertia platform is based on Texas Instruments CC2538 System-On-Chip microcontroller and integrates two IEEE 802.15.4-compatible wireless transceivers working in the 863-950 MHz and 2.4 GHz radio bands [21]. On this platform runs the

[2]Containing a large amount of sensors in the array can be helpful for various purposes: (a) to select those with optimal characteristics, (b) to find alternative sensors when some of them present malfunction, (c) to provide self-validation by observing the simultaneous response of multiple sensors, (d) to enable future implementation of multiple materials and their modifications toward the detection of multiple gases, and (e) to allow deeper signal processing and mathematical statistics such as cellular nonlinear networks [20].

[3]https://zolertia.io/product/re-mote/

Contiki operating system. The sensing subsystem, the Zolertia platform, and the Raspberry Pi are powered by an external power bank. Fig. 2 shows the entire system in the deployment field.

IV. Data aggregation

The nanosensors generate a large amount of data which can be spatially and temporally correlated. The data have to be meaningfully aggregated before they are transferred to a control station, so as not to congest the network. In chemical industries and in environments where chemical exposure may cause a health hazard to employees, different safety conditions are specified. The American Conference of Governmental Industrial Hygienists[4] (ACGIH) [22], [23] defines the **Threshold Limit Values** (TLV) as an exposure limit "to which it is believed nearly all workers can be exposed day after day for a working lifetime without ill effect". Similarly, it defines the **Threshold Limit Value Ceiling** (TLV-C) as "the concentration that should not be exceeded during any part of the working exposure." The first refers to a long-term exposure and requires a long-term sensing. In this case, the sensing system should sample all the sensors periodically and store the data for long-term analysis. These data are also useful for the study of long-term pollution. TLV-C, on the other hand, refers to short-term exposure and requires an alarm to be fired immediately when a set threshold is crossed. For the second type of sensing, the system's response time is a critical performance metric. It is affected by the sensors' response time as well as the end-to-end packet transmission delay. The nominal time is between 20 to 30 seconds, but most oil refineries set an upper limit of 60 seconds [2], [24].

The data aggregation strategy has a direct bearing on the reliability of the system, the network's traffic density, the packet transmission latency, and the lifetime of the network. If raw data are streamed directly, this will incur a high communication cost and a considerable latency. Aggregating data as they propagate towards the control station, on the other hand, reduces unnecessary redundancy and network traffic but introduces uncertainty during analysis.

In selecting the best aggregation strategy, we are faced with two challenges: Firstly, since the nanosensors are sensitive, their outputs fluctuate even in the absence of a gas. To establish the statistics of this error, at each sampling interval, we can take the output of each element of the sensor array as the outcome of a random experiment. Secondly, when a gas leak occurs, the perceived intensity varies due to a change in the spatio-temporal distribution of the gas molecules. A distinction between the authentic and the spurious fluctuations is critical during data aggregation. A simple averaging of the sixty-four nanosensors at a node level introduces bias towards extreme values and abstracts the variation in the fluctuation. We chose to employ the **min** and **max** operations at each sampling interval to ensure reliable and safe monitoring. The **min** operation minimizes the possibility of overlooking a gas leak (i.e., false negative is minimized). If the minimum of the samples is above a set threshold, then we have every reason to trust the sensor node. The **max** operation, on the other hand, minimizes the possibility of overreacting (false positive).

The uncertainty with which a gas leak is detected depends on the variance in the sampled values. Hence, it is vital to examine the variance arising from the **min** and **max** operations. Since the outputs of the nanosensors fluctuate in time as well as at an instance, we can regard them as random variables. The results of the **min** and **max** operations should likewise be regarded as random variables. The variances of these random variables encode our uncertainty in the aggregation task.

A. Aggregate Probability Density Function

The **min** operation compares the values of all the sensors and selects the one which is the minimum. In case of only two sensors reporting, it is expressed as:

$$\mathbf{s} = \begin{cases} \mathbf{s}_1 & \text{if } \mathbf{s}_1 \leq \mathbf{s}_2 \\ \mathbf{s}_2 & \text{if } \mathbf{s}_1 > \mathbf{s}_2 \end{cases} \tag{1}$$

For our case (with sixty-four nanosensors), we have the following relation:

$$\mathbf{s} = \mathbf{min}\left(\mathbf{s}_1, \mathbf{s}_2, \ldots \mathbf{s}_n\right) \tag{2}$$

Since $\mathbf{s}$ is a random variable by virtue of all its inputs being random variables, it is important to establish its statistics. We begin with its PDF:[5]

$$F\left(s\right) = P\left\{\mathbf{s} \leq s\right\} = P\left\{\mathbf{min}\left(\mathbf{s}_1, \mathbf{s}_2, \ldots \mathbf{s}_n\right) \leq s\right\} \tag{3}$$

Equation 3 is simpler to evaluate if we consider its complement, namely,

$$F\left(s\right) = 1 - P\left\{\mathbf{s} > s\right\} \tag{4}$$

in which case, we have:

$$F\left(s\right) = 1 - P\left\{\mathbf{min}\left(\mathbf{s}_1, \mathbf{s}_2, \ldots \mathbf{s}_n\right) > s\right\} \tag{5}$$

The right term in Equation 5 describes a condition wherein all the sensors report a value greater than s:

$$F\left(s\right) = 1 - P\left\{\mathbf{s}_1 > s, \mathbf{s}_2 > s, \ldots \mathbf{s}_n > s\right\} \tag{6}$$

Statistically speaking, the nanosensors are independent of one another, so that:

$$F\left(s\right) = 1 - P\left\{\mathbf{s}_1 > s\right\} P\left\{\mathbf{s}_2 > s\right\} \ldots P\left\{\mathbf{s}_n > s\right\} \tag{7}$$

Or:

$$F\left(s\right) = 1 - \prod_{i=1}^{n}\left(1 - P\left\{\mathbf{s}_i \leq s\right\}\right) = 1 - \prod_{i=1}^{n}\left(1 - F_i\left(s\right)\right) \tag{8}$$

where $F_i\left(s\right)$ is a PDF describing the output of the i-th sensor. With Equation 8 in place, we can derive the probability density function as follows:

$$f\left(s\right) = \frac{d}{ds}F\left(s\right) \tag{9}$$

[4]https://www.acgih.org/

[5]A Probability Distribution Function (PDF) is defines as: $F\left(\mathbf{s}\right) = P\left\{\mathbf{s} \leq s\right\}$, where $\mathbf{s}$ is a random variable and s is a real number.

When a node applies the **max** operator, it chooses the maximum value, so that its output as a random variable is expressed as:

$$\mathbf{s} = \mathbf{max}\left(\mathbf{s}_1, \mathbf{s}_2, \ldots \mathbf{s}_n\right) \tag{10}$$

The distribution function of this operation is expressed as follows:

$$F\left(s\right) = P\left\{\mathbf{s} \leq s\right\} = P\left\{\mathbf{max}\left(\mathbf{s}_1, \mathbf{s}_2, \ldots \mathbf{s}_n\right) \leq s\right\} \tag{11}$$

Following similar steps as in Equations 7 and 8, we can determine the PDF of this random variable as follows:

$$F\left(s\right) = \prod_{i=1}^{n} F_i\left(s\right) \tag{12}$$

B. Mean and Variance

In order to demonstrate how data aggregation affects the mean and variance of the output, we consider a normal condition in which a fluctuation in sensed data arises due to noise. We consider two theoretical cases, namely, when the noise is (a) uniformly distributed and (b) exponentially distributed. When the noise is uniformly distributed, it is possible to normalize the values so that its domain lies between 0 and 1. Hence, given the noise a nanosensor experiences can be considered as a uniformly distributed random variable, U(0,1), its PDF is given as:

$$F_i\left(s\right) = \int_0^s du = s \tag{13}$$

Likewise, given an exponentially distributed random variable, its PDF is expressed as:

$$F_i\left(s\right) = \int_0^s \lambda e^{-\lambda u} du = 1 - e^{-\lambda s} \tag{14}$$

λ, which is the inverse of the mean of the random variable, is called the rate of the process. When the noise PDF is uniformly distributed, Equation 8 yields:

$$F(s) = 1 - \left(1 - s\right)^n \tag{15}$$

1) **min***: Uniform Distribution:* With the statistics of the individual nanosensors in place, the **min** operation yields an aggregated PDF of (using Equation 8):

$$F(s) = 1 - \left(1 - s\right)^n \tag{16}$$

The corresponding density function is:

$$f\left(s\right) = \frac{d}{ds} F\left(s\right) = n\left(1 - s\right)^{n-1} \tag{17}$$

With $f(s)$ in place, we can compute the mean and the variance of the output of the **min** operation for the uniform distribution:

$$E\left[\mathbf{s}\right] = \int_0^1 s f\left(s\right) ds = n \int_0^1 s(1-s)^{n-1} ds \tag{18}$$

If we let $u = (1 - s)$ and substitute terms we get:

$$E\left[\mathbf{s}\right] = n \int_0^1 \left(1 - u\right) u^{n-1} du = 1 - \frac{1}{1 + 1/n} \tag{19}$$

Note that we started by assuming a normal condition where there was no gas leak. In which case, the node should produce no output. So, as we aggregate the outputs of the nanosensors, the mean approaches zero, unlike the case of the mean of the individual nanosensors which is 1/2. The variance of **s**, σ_s^2, is expressed as: $E\left[\left(\mathbf{s} - E\left[\mathbf{s}\right]\right)^2\right]$. Alternatively, it can be expressed as: $E\left[\mathbf{s}^2\right] - \left(E\left[\mathbf{s}\right]\right)^2$. Taking the latter expression yields:

$$\sigma_{min}^2 = \frac{1}{1 + 2/n} - \left(\frac{1}{1 + 1/n}\right)^2 \tag{20}$$

As can be seen, the variance as a result of data aggregation approaches zero, which means the confidence associated with the aggregated statistics is high.

2) **min***: Exponential Distribution:* Similarly, when the noise is exponentially distributed, Equation 8 yields:

$$F(s) = 1 - \left(1 - \left(1 - e^{-\lambda s}\right)\right)^n = 1 - e^{-\lambda n s} \tag{21}$$

The corresponding density function is:

$$f\left(s\right) = \lambda n e^{-\lambda n s} \tag{22}$$

Computing for the mean yields $E\left[\mathbf{s}\right] = 1/\lambda n$. Here, too, since the mean operation always favors the minimum value, as the array size increases, the mean of the aggregation output approaches zero (as it should be, since we are considering a normal condition). Similarly, the variance of this output is given as:

$$\sigma_{min}^2 = \left(\frac{1}{\lambda n}\right)^2 \tag{23}$$

3) **max***:* Here we consider the case when the noise is uniformly distributed, in which case:

$$F\left(s\right) = s^n \tag{24}$$

The pdf of **s** is:

$$f\left(s\right) = n s^{n-1} \tag{25}$$

The mean of this operation is given as:

$$E\left[\mathbf{s}\right] = \frac{1}{1 + 1/n} \tag{26}$$

The **max** operation favors the maximum value. If the magnitude of this value is less than a set threshold, it means that the possibility of experiencing a false positive is very small. As in the case of the **min** operation, here as well the variance approaches zero as a result of data aggregation:

$$\sigma_{max}^2 = \frac{1}{(n+1)^2(n+2)} \tag{27}$$

V. Network

To investigate the scope and usefulness of a wireless sensor network for monitoring toxic gases, we deployed 21 sensor nodes in an open field next to the Faculty of Computer Science (TU Dresden). Four of the nodes integrated arrays of ammonia nanosensors, whereas the rest were used as intermediate nodes to forward packets. The network had a grid topology and the ammonia sensors were placed at each of the four corners of the grid. Furthermore, a base station at one side of the network interfaced the sensor network with a nearby laptop computer. The Raspberry Pi boards attached to each of the nodes were

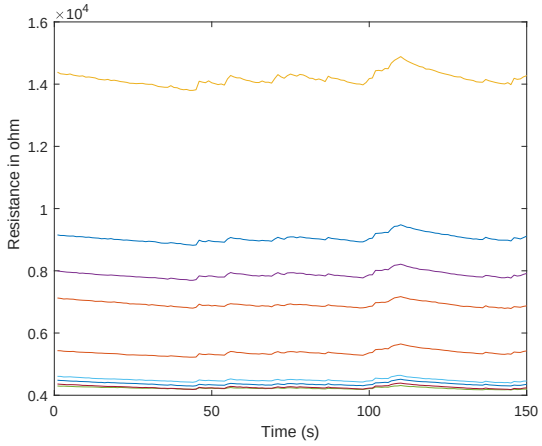

Fig. 3: The difference in the raw values of nine arbitrarily selected sensors of an array in the absence of ammonia.

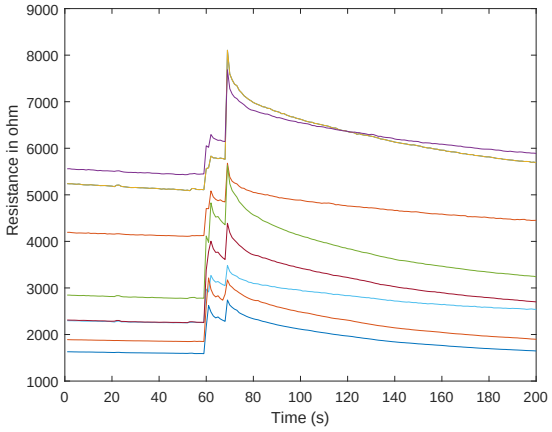

Fig. 4: The difference in the raw values of nine arbitrarily selected sensors of an array in the presence of ammonia (right).

tasked with collecting performance related statistics from the Zolertia platforms. In addition, they established a local area network to coordinate the experiments. The sensor nodes were configured to transmit packets in the 2.4 GHz radio band using 7 dBm transmission power. Each node transmitted packets at 1 Hz rate, the packets containing the **min**, **max**, and average values reflecting the observations of the 64 on-board nanosensors. In all, we conducted 100 independent experiments to evaluate the performance of the network.

A. Sensing

During our field deployment three of the gas sensors were not exposed to ammonia, but one of them (Node 2) was placed next to a bottle (ca. 5 cm away) containing ammonia. The lead of this bottle was removed for ca. 30 s during each experiment. The experiment took place under normal atmospheric condition (airflow: ca. 6 L/min, outside temperature: ca. 25°C, relative humidity: ca. 25%).

The nanosensors exhibited an appreciable difference in their zero-offset threshold, but in terms of their precision and accuracy, they were comparatively similar. Fig. 3 shows the outputs of nine arbitrarily selected nanosensors from a single array in the absence of ammonia. It is worth to mention that even though the dielectrophoretic deposition process was the same for all the 64 sensors of an array, the difference in their response was likely due to the presence of small unavoidable defects at the microelectrodes [17]. This feature remains, by and large, stable, though, in the presence of ammonia, as can be seen in Fig. 4.

Fig. 5 illustrates the difference in the raw values between the **min** and the **max** operations of the four nodes during the monitoring of ammonia for a sampling duration of 200 s. In each sampling interval a node performs the two operations by comparing the outputs of all the sixty-four nanosensors. For reasons we have not yet established, several sensors reported suspicious outputs which were not included during data aggregation. Except Node 2, all the others were monitoring a normal condition (the absence of a toxic gas).

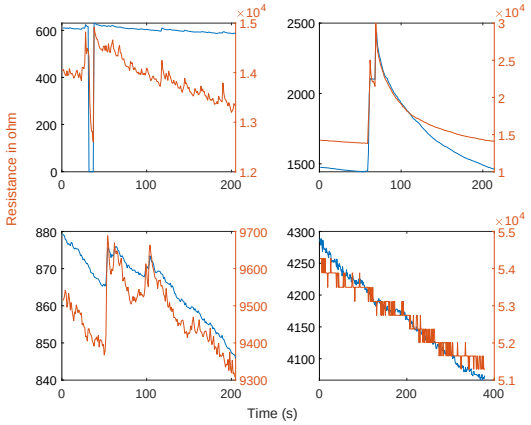

Fig. 5: Comparison of raw values of **min** and **max** operations. Except Node 2, the other nodes were not exposed to ammonia.

When regarded separately, the samples of both the **min** and **max** operations show appreciable fluctuations as do the raw data from the sensors, but the magnitude of fluctuations tend to disappear when the outputs of the two operations are compared, as can be seen in Fig. 6, where we plotted the histograms of the aggregated data. This feature affirms the theoretical assertion that the variances of both operations approach zero as the number of sensors increases, regardless of the statistical characteristics of the outputs of the individual sensors.

B. Routing

Multi-hop Routing is supported in two steps. In the first step, the topology of the network is established and represented by a binary adjacency matrix. How this is accomplished is explained in detail in [25]. As a summary, in this step, nodes discover and keep a list of their neighbours (including their hop-distance). For the size of our network, this step takes ca. 1.6 s.

Avoiding congestion and minimising packet loss is critical for toxic gas detection. To achieve these goals, firstly, a node uses unicast communication to send a packet to exactly one

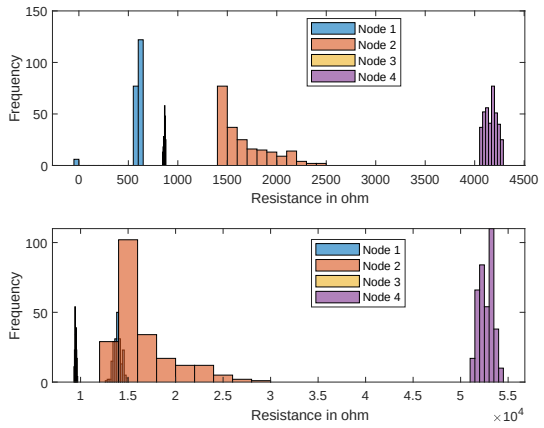

Fig. 6: Comparison of the histograms of the **min** and **max** operations. Only Node 2 was exposed to ammonia.

neighbour which is at least one-hop nearer to the sink. This takes place as long as packets are duly acknowledged. If a packet is lost, a node attempts to retransmit it twice; if both attempts fail, then it broadcasts the packet to all its neighbours and any receiving node, provided it is either the same hop-count away from the sink as the transmitter or at least one hop nearer to the sink, forwards this packet. Secondly, nodes perform local comparison before they decide to include a piece of data in a packet they transmit. The comparison consists of (i) freshly received values from neighbours, (ii) freshly computed local values, and (iii) values from the previous round. If the new *min* is not less than the *min* from the previous round, the node does not forward it. If, however, a new *min* is observed, then this will be transmitted along with the ID of the node which reports it. In addition, the node locally stores this value, regardless of where it originated. The same is true for the *max* and the *average* values. Algorithm 1 summarises this process for the **min** and **max** operations. An exception to this rule is an emergency situation. An emergency situation is flagged when a node locally detects that a concentration threshold is crossed, in which case the packet is directly forwarded towards the sink.

Local comparisons take place at 1 s interval. The short-range radio supported by the CC2538 System-On-Chip has a nominal transmission rate of 250 Kbps, but it rarely achieves this rate. If we assume a modest transmission rate of 100 kbps, the transmitter needs ca. 2.5 ms to transmit a packet of 28 bytes (the longest packet containing a *min*, *max*, and *average* values). If neighbours require on average 10 ms to win the medium – in the Time Slotted Channel Hopping (TSCH) protocol, the timeslot for the Zolertia platform is set 10 ms [26] –, then an intermediate node can collect up to 80 packets during the 1 s interval. In other words, the interval is long enough to collect packets from neighbours.

C. Link Quality

The quality of wireless links varies appreciably. We observed this phenomenon in different ways. Firstly, we measured the background noise at each node both before a packet

Algorithm 1: Processing min and max

Input : Received packets, local min, local max, past min, past max: $\mathbf{p}$, l_m, l_x, $m_{\tau-1}$, $x_{\tau-1}$
Output: Transmitted packet: p_{tx}
Aggregate *min*:
  $m_\tau \leftarrow \mathbf{min}\,(l_m, \mathbf{p}.m)$
  if $m_\tau < m_{\tau-1}$ **then**
    $m_{\tau-1} \leftarrow m_\tau$
    $p_{tx}.m \leftarrow m_\tau$
  else
    $p_{tx}.m \leftarrow NULL$
  end
end
Aggregate *max*:
  $x_\tau \leftarrow \mathbf{max}\,(l_x, \mathbf{p}.x)$
  if $x_\tau > x_{\tau-1}$ **then**
    $x_{\tau-1} \leftarrow x_\tau$
    $p_{tx}.x \leftarrow x_\tau$
  else
    $p_{tx}.x \leftarrow NULL$
  end
end

was transmitted and after a packet was received. Secondly, we measured the RSSI values of incoming ACK packets. Thirdly, we evaluated the statistics of successively received and lost packets to examine short-term link quality fluctuations. Fourthly, we compared the total number of packets a node successfully received with the total number of packets transmitted to the same node to determine long-term link quality fluctuations.

The IEEE 802.15.4 specification [27] defines a total of 16 channels in the 2.4 GHz band (numbered from 11 to 26). Each channel has a bandwidth of 2 MHz and is separated from neighbouring channels by a guard-band of 5 MHz. Some of these channels overlap with other ISM band channels and can be affected by nearby ISM networks (such as the LAN we established to monitor our experiments and other nearby WiFi networks) [28]. Therefore, not all channels are equally affected by surrounding noise and interference [29].

The background noise at the four gas sensors remained, by and large, stable in all the 16 available channels throughout our experiments. Fig. 7 displays the histogram of the background noise for Channel 25, which was the best for our setting. More than 95% of the time, it was below -90 dBm. Experiment results reveal that the Zolertia platform is capable of receiving a packet successfully if the RSSI value is above -90 dBm [30]. Consequently, the packet loss our network suffered was mainly due to packet collision or interference coming from other sources.

The packet success rate depends on the network traffic density and the surrounding cross technology interference (CTI). In this regard, we observed that the 16 available channels experienced different packet losses. To demonstrate this aspect, we flew an Unmanned Aerial Vehicle (UAV) during three of our experiments while the ground nodes transferred packets to the base station. Fig. 8 displays the performance of three

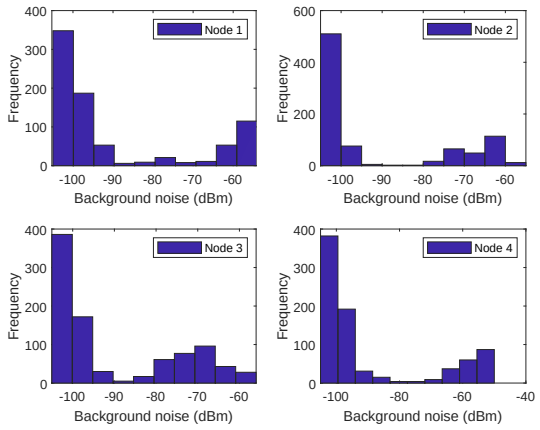

Fig. 7: The statistics of the background noise as perceived by the four sensor nodes integrating the arrays of gas sensors (Channel 25).

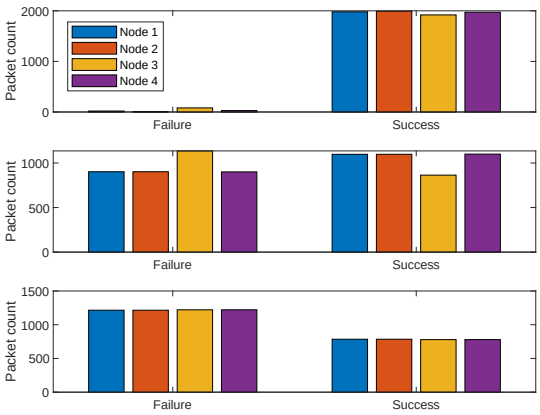

Fig. 8: Comparison of the total number of packets transmitted and the total number of packets received by the base station. The transmitters were the four nodes integrating the ammonia sensor arrays. The two nodes farthest away from the base station were each four-hop away and the two nodes nearest to the base station were each two-hop away. Top: Channel 25. Middle: Channel 26. Bottom: Channel 24.

adjacent channels (Channels 24, 25, and 26). The statistics we used to generate the histograms were based on the transfer of 2000 packets. As can be seen, Channel 25 performed best with more than 95% of the packets transferred successfully over the multihop links. The other channels, however, suffered a considerable packet loss on account of the CTI generated by the remote controller of the UAV.

D. End-to-End Latency

In order to measure the response time of the system, we set up a threshold of 40% relative resistance change (corresponding to ca. 5 ppm of ammonia) to trigger an alarm. Each node first aggregated the data from the sensors and then transmitted the result at 1 Hz rate. The system's response time consists of (1) the packet transmission end-to-end latency (which depends on the relative distance of the nodes from the base station) and (2) the time at which the nodes detect an interesting event.

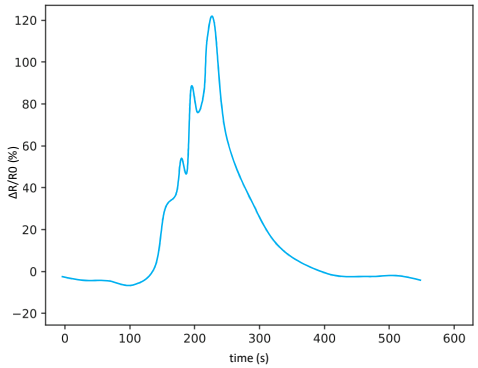

Fig. 9: Averaged sensing response ($\Delta R/R_0$) of the gas sensor array upon exposure to ammonia gas.

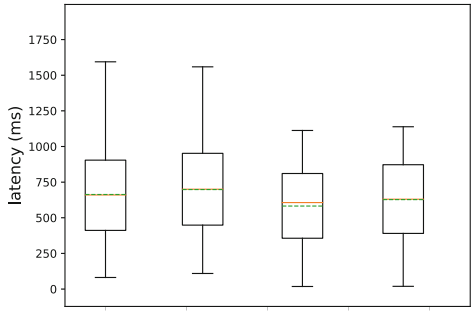

Fig. 10: The average end-to-end packet transmission latency of the four sensor nodes integrating the gas sensor arrays. The statistics were generated based on the reception of 2000 packets. The two left bars correspond to the nodes which were 4-hop away from the base station, whereas the two right bars correspond to the nodes which were 2-hop away from the base station.

Since we exposed only one of the nodes (Node 2, which was 2-hop away) to a concentration of ammonia due to safety concerns, we have to evaluate these two aspects separately. Fig. 9 shows the response of Node 2 to the concentration of ammonia to which it was exposed. (In plotting the response time of the nanosensor, we included a portion of raw data published elsewhere [31]. In the previous publication the focus was on the overall response time of a system involving a UAV, a mobile robot, a wireless sensor network, and a middleware. The size of the network was significantly smaller compared to the present case (5 vs 21) and the performance of the network was not analysed in detail. However, since the sensors' response time is independent of the network size or structure, including the response time of multiple experiments increases the statistical significance of the whole data.). The node needed ca. 100 s to cross the set threshold (based on the expected value of the **min** operation, as discussed in Sec. IV-B)[6]. Compared to commercially available ammonia sensors based on electrical readouts (a response time of ca. 2 to 3 min for 25-30 ppm concentration [32]), the response time

[6]We suspect that the actual response time of the sensor is smaller, but imperfect experimental conditions might have led to this observation.

is significantly small. Recently, Maity et al. [33] reported a paper electronics based solid state ammonia sensor with a response time of ca. 100 s for a sensitivity threshold of 10 ppm, which suggests that a single node responds with a high level of performance compared to the state of the art.

The average end-to-end communication delay for Node 2 was ca. 530 ms. Node 1, which was the same hop-away from the base station, experienced approximately the same average end-to-end latency. The other farther away nodes, Node 3 and Node 4, experienced an end-to-end latency of ca. 650 ms on average. Fig. 10 shows the box plot of the end-to-end communication latency for the 4 nodes. The green dash lines in the middle represent the mean value and the orange lines, the median.

VI. Evaluation

In Section II we demonstrated a wide range of applications that can be supported by wireless sensor networks monitoring dangerous or toxic gases. To evaluate the performance of our network we adopted the approaches used by Perez et al. [14] and Cheung et al. [8], in that we tested the reliability of the network in terms of (1) packet loss and end-to-end latency and (2) the response time of the entire system in the presence of a perceived danger. Packet loss and end-to-end latency are not aspects of the gas sensors and can be tested without the need to expose them to a concentration of a gas. The system's response, however, requires exposing the system to an actual concentration of a gas.

A. Packet Loss

Our experience with packet loss is similar to that of Perez et al. and Cheung et al. The difference is that they did not evaluate the performance of all the available channels, whereas we evaluated all the available channels. As we demonstrated in Fig. 8, the link quality was not the same for all the channels. Since the IEEE 802.15.4 communication band overlaps with other ISM bands, such as the ones used by wireless local area networks, the possibility of experiencing interference in the lower-end of the spectrum is high. As a result, in the literature Channel 26 is often favored for wireless sensor networks [34]–[36]. Our experience, however, suggests that this channel, too, can be affected by a strong cross technology interference. In all our experiments Channel 25 was the best. This suggests that dynamic channel selection is required to achieve the best performance.

B. Latency

Perez et al. achieved an end-to-end latency of 30 to 40 ms. Compared to what we achieved (ca. 530 to 650 ms), their performance appears to be impressive. But we need to carefully examine the deployment settings. Their network consisted only of 7 nodes, whereas ours consisted of 21 nodes. Secondly, they sampled the network at 1 m interval, whereas we sampled ours at 1 s interval. Therefore, the data traffic in the network for our case was considerably higher than theirs. This explains the relatively large amount of delay we experienced.

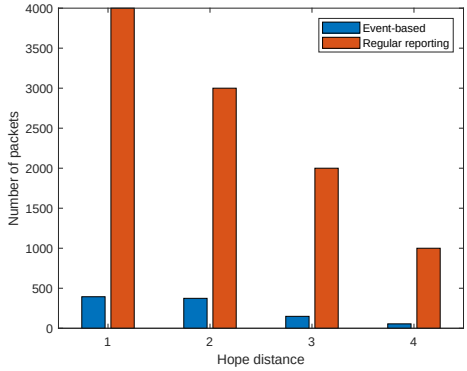

Fig. 11: The average number of packets intermediate nodes transmit in 1000 s. Red: Nodes transmit packets regularly at 1 Hz rate. Blue: Packet forwarding is event-based.

Similarly, Cheung et al. reported a system response time of 1-2 s, while the system response time for our case (the summation of the end-to-end latency and the time the node needed to detect the presence of ammonia) is ca. 101 s. The difference is considerable. One of the reasons for this is the difference in the network size. The network of Cheung et al. consisted of only 5 nodes and only one node communicated at a time. Moreover, our data aggregation strategy is more reliable, because Cheung et al. relied on a snapshot query (a single sample sufficed to fire an alarm), which is unreliable and liable to false positives an false negatives.

Having said this, the overall latency we experienced is well above the 60 s upper limit many chemical industries recommend to fire an alarm. Compared to the response time of the nanosensors, the contributions of the communication latency and the data aggregation are negligible (100 s vs. < 1s). This means that the response time of the nanosensors needs improvement and we are currently working on this aspect. This said, recently, we tailored the CNT surface towards selective sensing of hydrogen sulphide, achieving a response time below the required threshold of 60 s [17].

C. Packet Forwarding

Another aspect we investigate is the packet forwarding task of intermediate nodes. Assuming a child node communicates exactly with one parent node, in a regular routing protocol, a node d-hops away from the sink receives ca. $(d_{max} - d)p$ packets and forwards $(d_{max} - d + 1)p$ packets in a single round (where d_{max} is the farthest hop in the grid and p is the size of an ordinary data packet). These figures suggest that the packet transmission cost of the intermediate nodes near the sink increases linearly. For our case, packet forwarding is event-based. Furthermore, the evaluation of events occurs at two stages: locally and at an intermediate node, which significantly reduces the number of packets an intermediate node forwards to the sink. Fig. 11 compares the number of packets intermediate nodes forward on average in the two scenarios. The result was obtained analytically; the probability of events is taken to be exponentially distributed.

VII. Conclusion

In this paper we proposed a wireless sensor network for monitoring toxic gases. We developed arrays of nanosensors for monitoring ammonia and integrated them into wireless sensor nodes having communication, processing, and power subsystems.

We carried out a field deployment with a network of 21 sensor nodes. The network was forming a grid topology. The network was tasked with monitoring ammonia and the nodes were sampled at 1 Hz rate. The outputs of the arrays of sensors were locally aggregated using **min** and **max** operations and the packets were transferred to a central base station using multihop communications. Four of the 21 nodes integrated arrays of nanosensors, whereas the rest were employed as intermediate nodes. The four nodes with the ammonia sensors were placed at the four corners of the grid. We placed a bottle containing ammonia next to one of the nodes and removed the lid for ca. 30 s in each experiment. We set a 40% change in the total resistance of the nanosensors as the threshold to detect a concentration of ammonia which is large enough to trigger an alarm. The node required approximately 100 s to reach at a decision and trigger an alarm. We needed additional 700 ms to transfer a packet to the central station. Overall, with the selection of the best channel, the packet error rate of the network was below 5%.

Our future aim is to minimize the system's response time which, at presence, is higher than the limit prescribed by many chemical industries (which is 60 s).

References

[1] M. Y. Aalsalem, W. Z. Khan, W. Gharibi, M. K. Khan, and Q. Arshad, "Wireless sensor networks in oil and gas industry: Recent advances, taxonomy, requirements, and open challenges," *Journal of network and computer applications*, vol. 113, pp. 87–97, 2018.

[2] X. Chao, W. Dargie, and G. Lin, "Energy model for H2S monitoring wireless sensor network," in *2008 11th IEEE International Conference on Computational Science and Engineering*. IEEE, 2008, pp. 402–409.

[3] A. Valera-Medina, H. Xiao, M. Owen-Jones, W. I. David, and P. Bowen, "Ammonia for power," *Progress in Energy and combustion science*, vol. 69, pp. 63–102, 2018.

[4] E. Salzano, A. G. Agreda, A. Di Carluccio, and G. Fabbrocino, "Risk assessment and early warning systems for industrial facilities in seismic zones," *Reliability Engineering & System Safety*, vol. 94, no. 10, pp. 1577–1584, 2009.

[5] P. Zhao, Z. Li, X. Han, and X. Duan, "Supply chain network resilience by considering disruption propagation: Topological and operational perspectives," *IEEE Systems Journal*, 2022.

[6] H. Yilmazkuday, "Coronavirus disease 2019 and the global economy," *Transport Policy*, vol. 120, pp. 40–46, 2022.

[7] B. Zhang, Y. Liu, and S. Qiao, "A quantitative individual risk assessment method in process facilities with toxic gas release hazards: a combined scenario set and cfd approach," *Process safety progress*, vol. 38, no. 1, pp. 52–60, 2019.

[8] W.-F. Cheung, T.-H. Lin, and Y.-C. Lin, "A real-time construction safety monitoring system for hazardous gas integrating wireless sensor network and building information modeling technologies," *Sensors*, vol. 18, no. 2, p. 436, 2018.

[9] E. Broughton, "The bhopal disaster and its aftermath: a review," *Environmental Health*, vol. 4, no. 1, pp. 1–6, 2005.

[10] E. Commission, "Chemical accident prevention and preparedness," *MAH Bulletin*, no. 7, 2015.

[11] W. Dargie and C. Poellabauer, *Fundamentals of wireless sensor networks: theory and practice*. John Wiley & Sons, 2010.

[12] E. Llobet, "Gas sensors using carbon nanomaterials: A review," *Sensors and Actuators B: Chemical*, vol. 179, pp. 32–45, 2013.

[13] J. Chang, H. Meng, C. Li, J. Gao, S. Chen, Q. Hu, H. Li, and L. Feng, "A wearable toxic gas-monitoring device based on triboelectric nanogenerator for self-powered aniline early warning," *Advanced Materials Technologies*, vol. 5, no. 5, p. 1901087, 2020.

[14] C. Pérez-Garrido, F. J. González-Castano, D. Chaves-Diéguez, and P. S. Rodríguez-Hernández, "Wireless remote monitoring of toxic gases in shipbuilding," *Sensors*, vol. 14, no. 2, pp. 2981–3000, 2014.

[15] N. Asthana and R. Bahl, "IoT device for sewage gas monitoring and alert system," in *2019 1st International Conference on Innovations in Information and Communication Technology (ICIICT)*. IEEE, 2019, pp. 1–7.

[16] Y. A. Badamasi, "The working principle of an arduino," in *2014 11th international conference on electronics, computer and computation (ICECCO)*. IEEE, 2014, pp. 1–4.

[17] L. A. Panes-Ruiz, L. Riemenschneider, A. Chawa, M. Moner, M. Loeffler, B. Rellinghaus, R. Tetzlaff, V. Bezugly, B. Ibarlucea, and G. Cuniberti, "Selective and self-validating breath-level detection of hydrogen sulfide in humid air by gold nanoparticle-functionalized nanotube arrays," *Nano Research*, vol. 15, no. 3, pp. 2512–2521, 2022.

[18] S. Abbas, W. Yi, S. Yoo, A. Khalid, Z. Bhalli, J. Si, and X. Hou, "Highly efficient response of ammonia gas sensor based on surfactant-free sorted-semiconducting single-walled carbon nanotubes at room temperature," *physica status solidi (a)*, vol. 219, no. 7, p. 2100529, 2022.

[19] Q. Gu, Y. Ma, X. Chen, Z. Wu, F. Wang, H. Zhang, H. Zhou, G. Deng, and S. Zhou, "Sensing enhancement ammonia gas sensor based on a hybrid film fiber," *Optical Materials Express*, vol. 11, no. 12, pp. 3996–4006, 2021.

[20] S. Luo, Y. A. Samad, V. Chan, and K. Liao, "Cellular graphene: fabrication, mechanical properties, and strain-sensing applications," *Matter*, vol. 1, no. 5, pp. 1148–1202, 2019.

[21] I. 802.15.4, "Wireless medium access control (mac) and physical layer (PHY) specifications for low rate wireless personal area networks (lr-wpans)," 2003.

[22] R. Scott, *Basic concepts of industrial hygiene*. Routledge, 2018.

[23] M. J. Boss and D. W. Day, *Air sampling and industrial hygiene engineering*. CRC Press, 2020.

[24] H. Analytics, "Gas book," *Honeywell, Inc., Morristown, NJ*, p. 42, 2002.

[25] J. Wen and W. Dargie, "Dynamic topology construction in a joint deployment," *IEEE Sensors Journal*, vol. 22, no. 11, pp. 11 194–11 204, 2022.

[26] S. Duquennoy, A. Elsts, B. Al Nahas, and G. Oikonomo, "TSCH and 6tisch for contiki: Challenges, design and evaluation," in *2017 13th International Conference on Distributed Computing in Sensor Systems (DCOSS)*. IEEE, 2017, pp. 11–18.

[27] B. Mao, Y. Kawamoto, J. Liu, and N. Kato, "Harvesting and threat aware security configuration strategy for ieee 802.15. 4 based IoT networks," *IEEE Communications Letters*, vol. 23, no. 11, pp. 2130–2134, 2019.

[28] L. Polak and J. Milos, "Performance analysis of lora in the 2.4 ghz ism band: coexistence issues with wi-fi," *Telecommunication Systems*, vol. 74, no. 3, pp. 299–309, 2020.

[29] G. Cena, C. G. Demartini, M. G. Vakili, S. Scanzio, A. Valenzano, and C. Zunino, "Evaluating and modeling ieee 802.15. 4 TSCH resilience against wi-fi interference in new-generation highly-dependable wireless sensor networks," *Ad Hoc Networks*, vol. 106, p. 102199, 2020.

[30] J. Wen and W. Dargie, "Characterization of link quality fluctuation in mobile wireless sensor networks," *ACM Transactions on Cyber-Physical Systems*, vol. 5, no. 3, pp. 1–24, 2021.

[31] U. Aßmann, M. Belov, T.-T. T. Cong, W. Dargie, J. Wen, L. Urbas, C. Lohse, L. A. Panes-Ruiz, L. Riemenschneider, B. Ibarlucea *et al.*, "Sniffbots to the rescue–fog services for a gas-sniffing immersive robot collective," in *European Conference on Service-Oriented and Cloud Computing*. Springer, 2022, pp. 3–28.

[32] A. Maity and B. Ghosh, "Fast response paper based visual color change gas sensor for efficient ammonia detection at room temperature," *Scientific reports*, vol. 8, no. 1, pp. 1–10, 2018.

[33] A. Maity, A. Raychaudhuri, and B. Ghosh, "High sensitivity nh3 gas sensor with electrical readout made on paper with perovskite halide as sensor material," *Scientific reports*, vol. 9, no. 1, pp. 1–10, 2019.

[34] F. Domínguez, A. Touhafi, J. Tiete, and K. Steenhaut, "Coexistence with wifi for a home automation zigbee product," in *2012 19th IEEE Symposium on Communications and Vehicular Technology in the Benelux (SCVT)*. IEEE, 2012, pp. 1–6.

[35] Z. Wang, L. Kong, X. Liu, and G. Chen, "Embracing channel estimation in multi-packet reception of zigbee," *IEEE Transactions on Mobile Computing*, 2021.

[36] C. Shao, Y. Kim, and W. Lee, "Zero-effort proximity detection with zigbee," *IEEE Communications Letters*, vol. 24, no. 9, pp. 2047–2050, 2020.